Semicond. Sci. Technol. **26** (2011) 083001 (18pp) doi:10.1088/0268-1242/26/8/083001

**TOPICAL REVIEW**

# Applications of two-photon processes in semiconductor photonic devices: invited review

**Alex Hayat, Amir Nevet, Pavel Ginzburg and Meir Orenstein**

Department of Electrical Engineering, Technion, Haifa 32000, Israel

E-mail: nevet@tx.technion.ac.il

Received 31 January 2011, in final form 9 May 2011
Published 8 June 2011
Online at stacks.iop.org/SST/26/083001

**Abstract**

Semiconductor photonics is an advanced field, both from fundamental and applicative points of view, aimed at the integration of the unique features of optical communications and quantum optics with the miniaturization and controllability of semiconductors. Many classical and quantum applications may benefit from interaction between optical signals, usually implemented by nonlinear optical processes of various orders. The efficiency of such processes in semiconductors is being constantly enhanced, assisted by the progress in ultrashort laser pulses and ultra-sensitive detectors, enabling practical devices. In this review, the lowest order of nonlinear interactions—the two-photon processes in semiconductors—are discussed, and their applications to a variety of novel classical and quantum configurations are reviewed.

(Some figures in this article are in colour only in the electronic version)

## 1. Introduction

Applications based on semiconductor devices have been revolutionizing our everyday life since the invention of the transistor more than half a century ago, introducing miniature computational capabilities. Optics, the main carrier of the internet data, has been successfully integrated into semiconductors in terms of light sources, detectors and modulators; nevertheless it has not yet been able to introduce a significant alternative to electronics for signal processing and computing. Coulomb interaction between electrons at the core of electronic devices is much more significant than the weak nonlinear optical material-mediated interaction between photons, making electronic devices much simpler than their photonic counterparts. However, electronic devices such as transistors are based on charge carrier transport in semiconductors, which sets a fundamental limit on the operation speed. Nonlinear optical devices, on the other hand, are based on high-order transitions between energy levels that allow ultrafast signal processing. Moreover, while the strong interaction between charged particles causes fast decoherence, limiting quantum information applications, the weak interaction of photons with the environment makes them suitable for long-range interconnection and quantum communication applications.

In general, optical nonlinear interaction is described by the higher order terms of the macroscopic polarization $P$, which is given by a series of powers of the electrical field $E$:

$$P = \chi^{(1)}E + \chi^{(2)}E^2 + \chi^{(3)}E^3 + \cdots, \tag{1}$$

where the equation is in general a tensor equation. The scaling between the different orders of the polarization is on the order of the 'characteristic atomic field' $E_0$:

$$\chi^{(n+1)}/\chi^{(n)} \sim |E_0|, \quad |E_0| \sim \frac{e}{4\pi\varepsilon_0 a_0^2} \sim 5 \times 10^{11}\ \mathrm{V\,m^{-1}}, \tag{2}$$

where $e$ is the electron charge, $\varepsilon_0$ is the vacuum electrical permittivity and $a_0$ is the Bohr radius.

Such intense fields cannot be usually achieved at a single-photon level, meaning that any nonlinear optical process is expected to be relatively weak. However, there are various techniques to enhance the microscopic nonlinear optical processes by properly designing collective

 

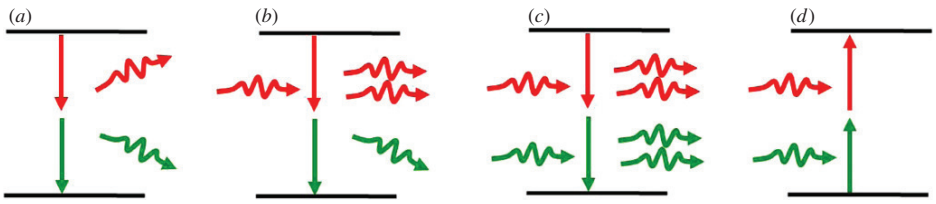


**Figure 1.** (*a*) Electron transition diagram of spontaneous TPE, (*b*) singly stimulated TPE, (*c*) fully (doubly) stimulated TPE (TPG) and (*d*) TPA.

macroscopic interaction. For all-optical nonlinear processes in transparent materials, where only optical fields interact and no free charge carriers are involved, multiple microscopic interactions should be aligned in phase, and therefore phasematched crystals or photonic cavities must be employed. In optoelectronic nonlinear processes that involve charge carriers, phasematching is not required, but the nonlinear process efficiency can still be enhanced by photonic structures that increase the local field intensity.

Interaction between photons is mediated by their mutual interaction with an electron. Understanding the fundamentals behind such quantum-mechanical phenomena can significantly improve the utilization of these nonlinear processes, often referred to as multi-photon processes. These processes are applied either in various all-optical schemes based on nonlinear interactions between optical fields yielding a 'photon in–photon out' configuration or in other optoelectronic schemes based on generation or detection of photons—involving free charge carriers as part of the input or output of the device. Some aspects of quantum information processing including quantum cryptography and imaging are inherently related to multi-photon detection, whereas high-efficiency room-temperature quantum sources of heralded single-photon and of entangled-photon pairs are related to multi-photon emission.

In this review we focus on applications of nonlinear optical processes in which electron transitions between real energy levels occur by emitting or absorbing a pair of photons. Spontaneous two-photon emission (TPE) is the process in which a transition from a higher level results in the simultaneous emission of two photons (figure 1(*a*)); singly stimulated TPE is caused by a photon with energy below the energy gap that stimulates an emission resulting in the duplication of the input photon and the spontaneous emission of a complementary photon (figure 1(*b*)); fully stimulated TPE employs two photons with sum-energy equal to the energy gap to stimulate the emission resulting in the duplication of the two input photons (figure 1(*c*))—a process that under the population inversion condition is the source of nonlinear two-photon gain (TPG). Two-photon absorption (TPA) is the opposite process to TPG, in which two photons are absorbed (figure 1(*d*)) rather than duplicated.

Another type of nonlinear process which may accompany the TPA mentioned above is sum-frequency generation (SFG), or second harmonic generation (SHG) in the degenerate case (equal input wavelengths), which occurs in noncentrosymmetric materials. Schematically, these two processes may be compared as follows.

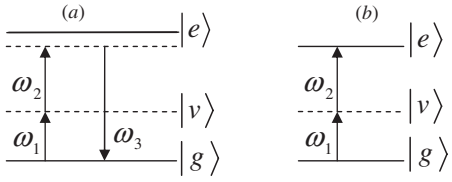


**Figure 2.** Scheme of (*a*) SFG and (*b*) TPA. $|g\rangle$ and $|e\rangle$ are ground and excited real levels respectively and $\langle v\rangle$ is a virtual level.

The main difference between the outcomes of these two processes is that the end product of SFG is the sum-frequency photon, while TPA results in a charge carrier at the excited state. The relative efficiencies of the processes are deduced by comparing the basic quantum-mechanical transition probabilities. The probability amplitude of SFG, proportional to the second-order nonlinear susceptibility $\chi^{(2)}$, is a third-order term in the perturbation theory:

$$M_{\mathrm{SFG}} \propto \chi_2 \varepsilon_3 \sim \sum_n \frac{\mu_{eg}\mu_{ne}\mu_{gn}\varepsilon_1\varepsilon_2\varepsilon_3}{(\omega_{eg}-\omega_1-\omega_2)(\omega_{ng}-\omega_1)} + \text{permutations}, \tag{3}$$

where the summation is performed over all possible intermediate states $|n\rangle$, forming the virtual state $|v\rangle$ (figure 2). $\mu_{ij}$ and $\hbar\omega_{ij}$ are the $i$ to $j$ level transition dipole moment matrix element and energy difference respectively, $\varepsilon_i$ is the photon field, while $\omega_1$ and $\omega_2$ are the radial frequencies of the photons participating in the process.

Generally, in transparent nonlinear crystals, energy separation between the real quantized states of the system (solid lines in figure 2) is largely detuned from the incident and generated photon energies to prevent absorption. Moreover, SFG is a coherent all-optical process, meaning that in order to achieve macroscopic efficiency, the phasematching conditions should be fulfilled:

$$\Delta k = k_3 - k_2 - k_1 = 0, \tag{4}$$

which is the momentum conservation of photon momentum only, namely $k_3, k_2, k_1$. To fulfill the phasematching conditions, birefringent crystals or various types of quasi-phasematching techniques may be used. All the above make applications based on SFG relatively bulky, since interaction distances longer than hundreds of wavelengths are required to achieve a significant signal at the output.

For certain applications, such as infrared (IR) photon detection, optical output is not required, and a more convenient process of TPA may be used. The TPA rate is given by

$$R_{\mathrm{TPA}} = 2\pi \left(\frac{e}{\hbar}\right)^4 |M_{\mathrm{TPA}}|^2 \, \delta\left(\omega_0 - \omega_1 - \omega_2\right), \tag{5}$$

where the matrix element is given by the second-order term in the perturbation theory:

$$M \sim \sum_n \left( \frac{\mu_{en}\mu_{ng}\varepsilon_1\varepsilon_2}{\omega_{ng} - \omega_1} + \frac{\mu_{en}\mu_{ng}\varepsilon_1\varepsilon_2}{\omega_{ng} - \omega_2} \right). \quad (6)$$

The simplest comparison between the order of magnitude of SFG and TPA can be done by comparing the rate of SFG related to the square of equation (3), to the rate of TPA related to the square of equation (6). Being a resonant second-order process in the perturbation theory, carrier-generating TPA is therefore preferable to the all-optical third-order SFG in optoelectronic devices where no optical output is needed, with an additional advantage of not requiring phasematching.

The difference between the perturbation orders and nonlinear susceptibility terms can be somewhat confusing. For example, $\chi^{(2)}$ is a second-order all-optical nonlinear susceptibility (equation 1); however, the probability amplitude of the process is calculated by the third-order term in the perturbation theory (equation 3). Similarly the linear first-order all-optical susceptibility $\chi^{(1)}$ is calculated by the second-order term in the perturbation theory. According to the optical theorem, there is a certain relationship between the imaginary part of an all-optical process of a given perturbation order and a process involving charge carriers with half of the perturbation order. The most well-known example is the Kramers–Kronig relationship between $\mathrm{Im}\left(\chi^{(1)}\right)$ (all-optical second-order perturbation) and one-photon absorption coefficient (first-order perturbation electron transition), while another example relates $\mathrm{Im}\left(\chi^{(3)}\right)$ (all-optical fourth-order perturbation) to TPA coefficient (second-order perturbation electron transition). Nevertheless, the strength of each process is calculated via the perturbation theory, yielding a one-photon absorption rate much higher than both $\chi^{(3)}$ four-wave mixing rate, and SHG rate. Similar calculations can show that TPE is a lower order more efficient alternative to parametric down-conversion (PDC) for photon pair generation in quantum information applications, while TPG in some applications can be an efficient electrically pumped counterpart of optical parametric amplification.

The structure of the review is as follows: in section 2, we discuss the application of TPA for ultrafast optical multiplication employed for pulse characterization in autocorrelators. The optical multiplication via TPA can also be employed for signal processing and logic—reviewed in section 3—and for quantum detectors—reviewed in section 4. Section 5 discusses the quantum technique of coherent control based on TPA. Section 6 describes spontaneous TPE in semiconductors, and section 7 presents stimulated semiconductor TPE and semiconductor TPG.

## 2. Autocorrelators based on TPA in semiconductors

Autocorrelation, the correlation between a signal and its duplication, is a tool employed in the analysis of statistical and temporal characteristics of a signal. Optical autocorrelation of a complex field $E(t)$, defined by $\int_{-\infty}^{\infty} E(t)\, E^*(t+\tau)\, \mathrm{d}t$, may be used to measure the spectrum of a light source or its coherence length, while optical autocorrelation of the field intensity $I(t) = |E(t)|^2$, defined by $\int_{-\infty}^{\infty} I(t)\, I(t+\tau)\, \mathrm{d}t$, may be used to measure its degree of second-order coherence and to estimate the duration of short pulses [1, 2]. Since electronic response is too slow to enable this measurement for ultrashort pulses, optical multiplication is needed. To generate multiplication between light intensities, a suitable nonlinear process may be exploited, enabling an interaction of a pulse with its delayed duplicate (figure 3(*a*)). In this method a train of laser pulses is split into two arms of a Michelson interferometer in which the pulses in one arm are delayed in respect to those in the other. The combined pulse trains propagate through a nonlinear element, and the detected signal is examined as a function of the time delay between the arms of the interferometer, $\tau$ (figure 3(*b*)). This signal is given by [3]

$$S(\tau) = 1 + 2G_2(\tau) + 4\mathrm{Re}[F_1(\tau)\mathrm{e}^{-\mathrm{i}\omega\tau}] + \mathrm{Re}[F_2(\tau)\mathrm{e}^{-2\mathrm{i}\omega\tau}], \quad (7)$$

where $G_2 = \int_{-\infty}^{\infty} I(t)\, I(t+\tau)\, \mathrm{d}t$ is the intensity autocorrelation signal and $F_1$ and $F_2$ are the interference terms (figure 3(*b*), inset). The interference terms can be either filtered out from the measured signal or avoided by employing a non-collinear geometry. The full-width half-maximum (FWHM) of $G_2$ determines the pulse duration assuming that its specific pulse shape is known.

SHG was used in the first autocorrelation measurements [4] and has remained the most commonly used optical autocorrelation method ever since. In the beginning of the 1990s, as the field of ultrashort pulse generation and characterization rapidly developed, an autocorrelator based on TPA in semiconductors has been proposed as an alternative for the SHG technique [5]. In this method the nonlinear crystal and detector are replaced by a single semiconductor detector (figure 4), transforming an optical signal directly into an electrical signal through the second-order transition of TPA. In TPA, the time interval between the photons in the absorbed pair is dictated by the Heisenberg uncertainty principle, $\hbar/E_g$ (where $E_g$ is the bandgap energy), which is a few fs in the optical range, therefore it is clearly suitable for ultrafast measurements.

TPA autocorrelators have many advantages over the SHG technique. SHG is a third-order process in the perturbation theory and requires phasematching between the inputs at a frequency $\omega$ and the product at $2\omega$ to allow momentum conservation, in order to increase its efficiency significantly and render it practical. TPA on the other hand is a resonant second-order transition in which only fields at the original frequency, $\omega$, are involved. Therefore, it is inherently more sensitive than SHG and allows characterization of extremely short pulses as it has a wide wavelength range of operation—not limited by the narrow phasematching bandwidth. The lack of phasematching requirement also makes TPA methods inexpensive and very easy to use and integrate in experiments, using readily available devices such as LEDs and photodiodes, whereas ultrashort pulse characterization by SHG requires crystals which are expensive

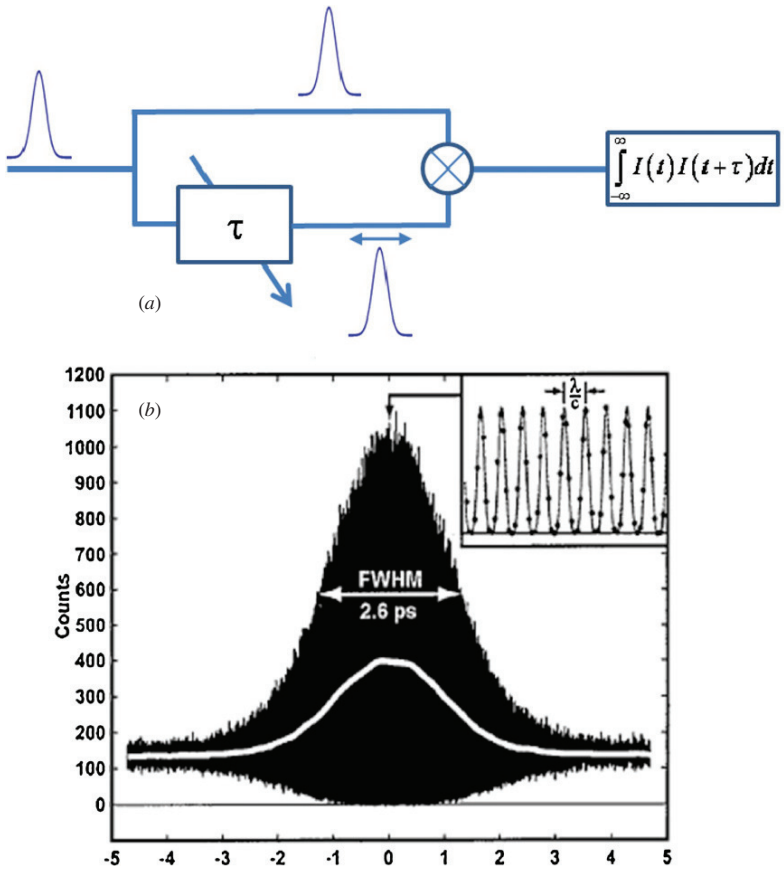


**Figure 3.** (*a*) Schematics of an autocorrelation implementation. (*b*) Measured interferogram of a collinear autocorrelation setup. The white continuous line representing the intensity interferometric term, $G_2$, is obtained by averaging. The inset shows the interference fringes of the interferogram (reprinted with permission from [24]).

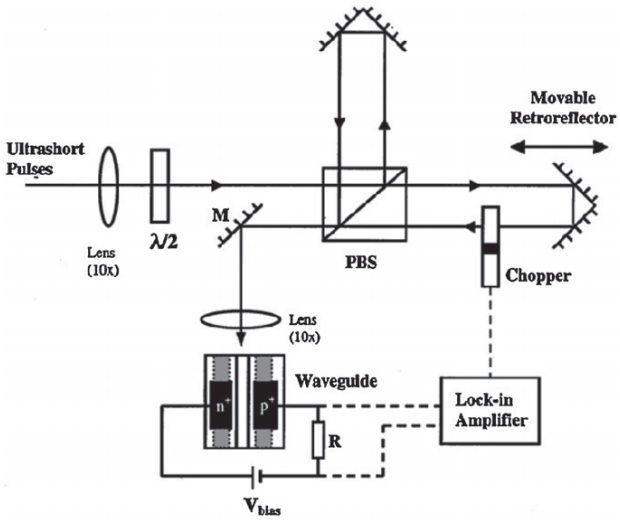


**Figure 4.** Interferometric autocorrelator setup based on a semiconductor waveguide and a lock-in amplifier (reprinted with permission from [11]).

and fragile, demanding delicate adjustment of the crystal tilt angle and temperature for the phasematching. Moreover, SHG is polarization sensitive, whereas TPA-induced current is almost insensitive to polarization [6].

The technique was first implemented for a wavelength of 1.91 $\mu$m using a commercial Si photodiode, and for a wavelength of 1.06 $\mu$m using a GaAsP photodiode and CdS photoconductive cell [5] at room temperature; however, the detection efficiency was relatively low. In order to enhance the effect of TPA, GaAs/AlGaAs waveguides were used [7, 8], resulting in enhanced detection efficiency due to the greater interaction length. This scheme was also demonstrated at the telecom wavelength of 1.55 $\mu$m incorporating lock-in amplifiers, utilizing the relatively high TPA coefficient of InGaAsP, generating current at an average-power peak-power product as low as $0.15 \times 10^{-3}$ $(\text{mW})^2$ [9, 10], and in Si waveguide, resulting in an average-power peak-power sensitivity of 1 $(\text{mW})^2$ [11], which is more sensitive than TPA in a Si avalanche photodiode (APD) [12].

Autocorrelation of pulses generated by Ti:sapphire at a wavelength of 800 nm was demonstrated in ZnSe [13] and in an ordinary off-the-shelf GaAsP photodiode down to a pulse width of 6 fs [14], exploiting the broad spectral response of TPA. It was also shown that the sensitivity of these techniques can be further improved by designing a microcavity structure [15]. In general, the variety of semiconductor devices enables

autocorrelation measurement by interband transition over the wide wavelength range of 0.7–3.6 $\mu$m, as is summarized in [16], and in the UV range of 140–280 nm [17]. By exploiting intersubband transitions in quantum wells (QWs), the regime of mid-IR can also be characterized [18, 19, 20, 21, 22]. This technique is based on two-photon transitions in QW IR photodetectors involving two bound subbands and one continuum resonance. In contrast to TPA-based detection, autocorrelation through two-photon luminescence may also be used, as was recently demonstrated for the investigation of the nonlinear absorption characteristics of a single InGaN/GaN quantum dot (QD) [23].

A breakthrough in TPA-based autocorrelator sensitivity was achieved by employing a commercial GaAs photomultiplier tube (PMT) as the detector of 1.5 $\mu$m signals [24] (see figure 5), suitable, in principle, to any wavelength between 900 and 1800 nm. The generated photoelectrons in such a detector are emitted from the semiconductor into vacuum and subsequently amplified by generating secondary emissions in multiple dynode stages. The setup exhibited a sensitivity of $1.7 \times 10^{-4}$ $(\mathrm{mW})^2$ with a very high dynamic range, enabling autocorrelation measurements of continuous wave (CW) light with average powers from $\sim$1 $\mu$W to 1 mW. Although CW light measurements of the 1.5 $\mu$m signal were achieved beforehand in Si APDs [25, 26], the sensitivity and dynamic range of these detectors are limited due to residual single-photon absorption, which is not observed in the PMT. This sensitive autocorrelation technique using a PMT recently enabled the measurement of bunching of photons emitted from chaotic sources on an ultrashort timescale [27], and was used for the demonstration of pulse compression by TPG [28]. Since TPA is intensity dependent, the photocurrent of the PMT is inversely proportional to the spot size of the optical beams, and therefore an improvement in sensitivity of an order of magnitude may still be achieved by this scheme if the PMT is designed to allow reduction of the spot size down to the diffraction limit [24].

A disadvantage of the TPA autocorrelators is that the detection erases any phase information and any asymmetries of the pulse, enabling extraction of pulse duration only, based on a preliminary assumption of its shape. The typical SHG autocorrelator gives the same information; however the fact that the product of the two input signals appears as an optical signal permits its spectral measurement in addition to its intensity detection. This feature is the basis for complete characterization of the input pulse by techniques such as frequency-resolved optical gating (FROG) and spectral phase interferometry for direct electric-field reconstruction (SPIDER) [29]. However, another technique very similar to FROG, the sonogram technique, in which a sonogram trace is generated by cross-correlating the pulse with a spectral slice of its replica, was shown to be suitable for implementation with TPA detection as well [30].

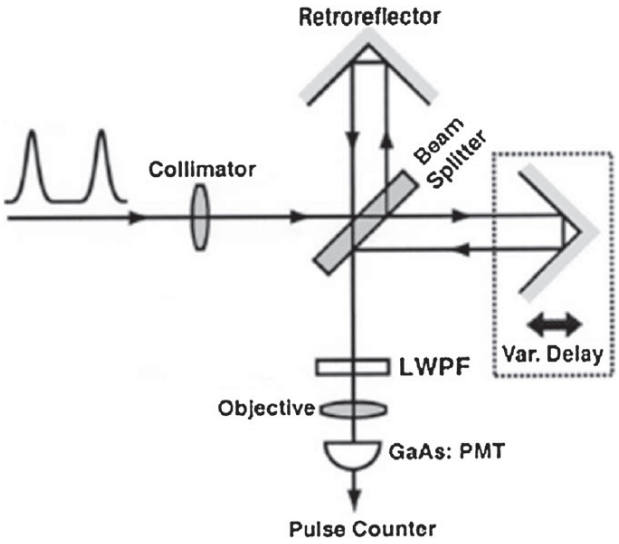


**Figure 5.** Interferometric autocorrelator setup based on GaAs PMT (reprinted with permission from [24]).

## 3. TPA-based signal processing

Optical signal processing can exploit the extremely wide bandwidth of the constantly expanding optical communication networks and provide a solution for the interconnect bottleneck in microelectronics. Signal processing including multiplexing, sampling and logic requires nonlinear operations such as multiplication of signals. The time response of the nonlinear element usually limits the speed of the signal processing, while the efficiency is determined by the strength of the nonlinearity. Various optical nonlinear processes were employed for all-optical switching and logic; however, all-optical nonlinear effects are based on high-order nonlinearities, making them less efficient, and require phasematching, which complicates the design and limits the bandwidth.

TPA is the lowest-order nonlinear process and does not require phasematching. Therefore it is a very efficient, fast and broadband nonlinearity. The rate of TPA is proportional to the product of two intensities (equations (5) and (6)), making this process suitable for optical signal multiplication. In most applications, optically processed signals are converted eventually into electrical ones, and thus using an all-optical multiplication results in a two-step process of optical nonlinearity followed by linear detection. On the other hand, in semiconductor TPA, nonlinear signal multiplication and detection are combined into one process, significantly simplifying the design and making it much more efficient. Considerable progress has been made in order to take advantage of TPA for optical signal processing in several applications.

### *3.1. Optical demultiplexing*

One of the widely employed techniques in optical communications to increase the number of channels is optical time domain multiplexing (OTDM), which uses short pulses to transmit data, where a specific time slot is allocated for each channel, so that signals from all the channels are interleaved in the transmission (figure 6).

The receiver in an OTDM system must be able to single out bits sent on a specific channel. A demultiplexing technique

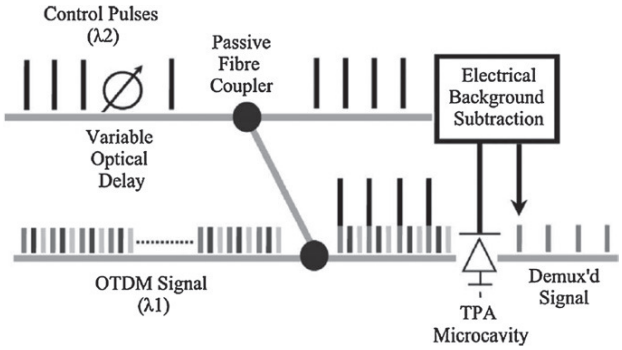


**Figure 6.** TPA-based OTDM demultiplexing (reprinted with permission from [32]).

based on semiconductor TPA was demonstrated allowing Tb $s^{-1}$ rates [31] based on the idea that a control optical pulse overlaps the bit-slot of the desired channel so that only a specific channel bit-slot will result in TPA detection, whereas the TPA detector is transparent to other channel bit-slots. In order to make the demultiplexer signal more stable, the control and the signal wavelengths are chosen sufficiently different to prevent interference. The multiplication by TPA is almost instantaneous, and the maximal switching rate is determined by the data and control pulse width in this scheme. In the experimental demonstration of TPA-based OTDM demultiplexing in an InGaAsP 1.3 $\mu$m Fabry–Perot laser diode, 500 fs optical pulses at 1.5 $\mu$m were used for the control and for the signal with relatively low peak powers of 10 and 1 W respectively, whereas the maximum bit rate of the individual channels in the OTDM system was limited to 2.5 Gb $s^{-1}$ by the electrical response of the diode. A microcavity-based TPA OTDM demultiplexer was also proposed [32], where the microcavity field enhancement can significantly boost the performance of the nonlinear scheme.

Another multiplexing technique was proposed by code-division multiple-access (CDMA), which exploits mathematical orthogonality between waveforms. In coherent short pulse optical implementation of CDMA, multiplexing is achieved by assigning phase codes to different transmitter–receiver pairs which stretches fs pulses into low-intensity ps ones. The receiver must detect waveforms corresponding to the desired code while rejecting the others by a matched phase-shaper followed by a nonlinear optical thresholder. The matching phase results in the reconstruction of a fs pulse which is singled out by the nonlinear thresholder, while the rest of the waveforms maintain low intensity and are not detected. A semiconductor TPA-based thresholder was implemented in a 0.6 $\mu$m GaAs layer sandwiched between $Al_{0.15}Ga_{0.85}As$ layers [33]. Pulses with ∼150 fs duration at 1.5 $\mu$m wavelength at 80 MHz repetition rate were used, stretched by a pulse-shaper up to 4 ps, and a TPA-induced photocurrent inversely proportional to the pulse duration was demonstrated.

### 3.2. Optical clock recovery

Synchronizing a clock to a data stream is crucial in any optical receiver or demultiplexer. The slow time response of electronic clock recovery can be overcome by employing optical multiplication in order to measure the timing between the optical data and clock, which can be inserted into a phase-locked loop (PLL) for synchronization. Various optical nonlinearities were used for optical clock recovery including four-wave mixing in fibers [34], in electro-absorption modulators [35], as well as other nonlinearities in electro-optic modulators [36]. However these nonlinearities are limited to a narrow wavelength range and are polarization sensitive. These limitations were eliminated in a semiconductor TPA-based optical clock recovery system demonstrated in a Si APD which significantly enhances the sensitivity [37] (figure 7). In the TPA-based scheme, the telecom-wavelength (1530–1570 nm) clock and data are combined on the surface of a Si APD with a 3 $\mu$m spot size resulting in a photocurrent proportional to the product of the data and the clock intensities. The pulse widths were around 30 ps at ∼2.8 mW average power with 12.5 Gb $s^{-1}$ repetition rate.

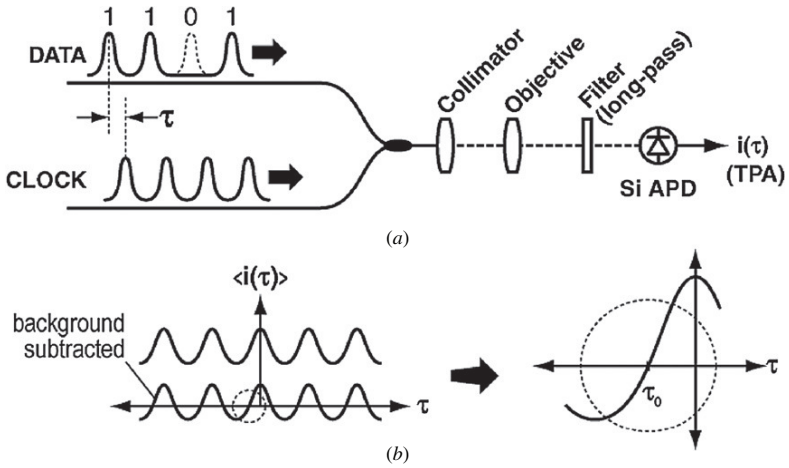


**Figure 7.**Si APD TPA-based data–clock time delay measurement setup (reprinted with permission from [37]).

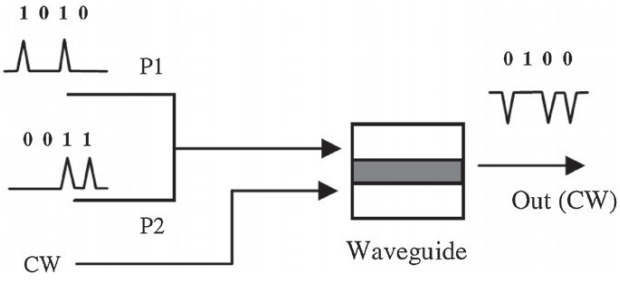


**Figure 8.** TPA-based NOR operation principle (reprinted with permission from [39]).

In this scheme, the time-averaged TPA-induced photocurrent is maximal when the time-aligned clock and data are temporally aligned, whereas misalignment results in an error signal. The background TPA signals resulting from the data and the clock alone are independent of the time delay and can be subtracted, while the remaining error signal can be fed into a PLL. It is interesting to note that the measured bit-error rate showed no appreciable power penalty resulting from the clock recovery relative to back-to-back with the original clock. A later experiment based on a similar TPA-based demonstrated clock recovery at repetition rates as high as 80 Gb $s^{-1}$ with 4 ps wide pulses at several mW average power [38].

### *3.3. TPA all-optical logic*

Digital ultrafast all-optical signal processing as well as routing in optical networks requires all-optical logic gates. The principle of implementing the simple NOT gate by TPA is based on combining a pump pulse and a CW probe beam at different wavelengths in a TPA device, so that only the sum of the pump and the probe energies is larger than the bandgap energy suitable for TPA, with no one-photon absorption of the pump or the probe alone. In such a configuration, a pulse in the pump beam will result in a dip in the probe beam caused by TPA, corresponding to the NOT operation. A two-input NOR gate can be constructed in a similar manner where the dips in the probe are caused by either of the inputs or both (figure 8).

A NOR gate based on the above concept was implemented in a $Si/SiO_2$ waveguide that allows tight optical mode confinement for intensity enhancement [39]. In that experiment the waveguide was 10 mm long, 220 nm high and 480 nm wide. Pump pulses with 1.6 ps width and 5 W peak power were used. This resulted in nearly 90% extinguished probe power from less than 20 mW CW level at the telecom wavelength of 1560 nm. In order to implement two distinguished inputs into the NOR gate and prevent interference, a 50 nm wide pulse was spectrally divided into 1545 and 1555 nm central wavelength pulses at an 80 Gb $s^{-1}$ data rate.

Another somewhat slower all-optical logic is based on the TPA-induced carrier population effect on the refractive index in semiconductor microcavities. In a high-quality microcavity, modulation of the index by pump TPA-induced carriers can tune a specific wavelength probe in or out of the cavity resonance resulting in drastic change in the transmission of the probe.

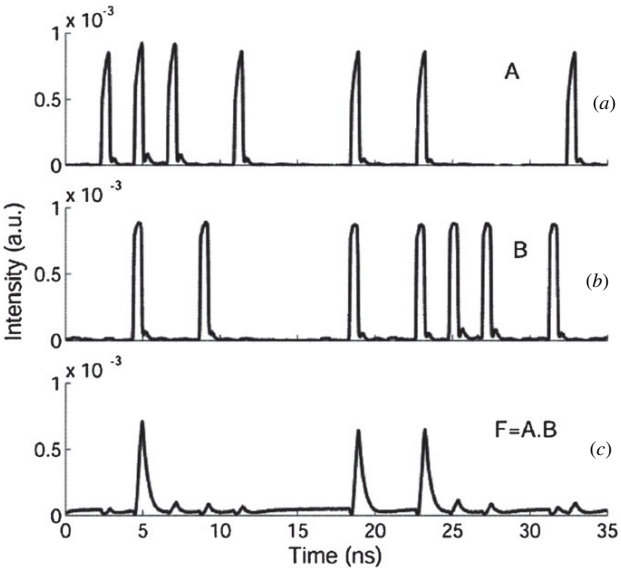


**Figure 9.** Time traces showing an AND gate: (*a*) 'A' and (b) 'B' are the two input pumps tuned to the resonance at 1550 nm and (*c*) 'F = A.B' is the output probe signal tuned to the next higher resonance at 1560 nm (reprinted with permission from [40]).

The nonlinearity in this case is comprised of both the TPA and the nonlinear effect of the index on the cavity transmission. Therefore, despite the almost instantaneous TPA, the carrier population modulation is slower than a ps, resulting in much more efficient but slower logic than pure TPA-based schemes. Optical AND and NAND gates were implemented in 0.5 $\mu$m × 0.5 $\mu$m cross-section, 10 $\mu$m radius GaAs and InP ring resonators with 500 MHz repetition rate, operated with 500 ps, 1550 nm central wavelength pulses with a 10 mW CW probe at 1560 nm [40] (figure 9). Similar concepts were implemented in Si photonic circuits for optical AND and NAND gates by micro-ring resonators operated with 200 ps pulses at a 310 Mbit $s^{-1}$ repetition rate and 2 mW coupled average power resulting in an ∼10 dB extinction ratio [41]. A NOR gate based on two symmetric GaAs–AlGaAs micro-ring resonators was demonstrated with a switching energy of the gate of 20 pJ/pulse [42].

## 4. Quantum detectors based on semiconductor TPA

Fiber-optic quantum communications use near-IR photons at the wavelength range of 1.3–1.6 $\mu$m for which single-photon detectors are based on narrow-bandgap InGaAs/InP APDs suffering from low efficiency and high dark count (DC) rates. Moreover, in order to reduce the effect of DC these detectors are usually operated in gated mode, with bit-rates limited to less than a MHz by the relatively high afterpulsing rate in these detectors. Wider bandgap materials have a much lower DC rate and do not require gating; however they cannot be applied directly to the telecom-wavelength range. Up-conversion of a single photon to shorter wavelengths to be detected by a Si

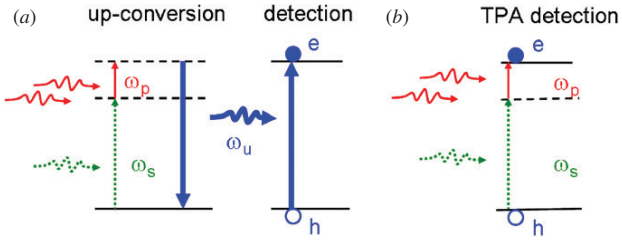


**Figure 10.** (*a*) Detection via up-conversion followed by one-photon absorption; (*b*) detection via TPA. The solid horizontal lines represent electron energy levels and the dashed lines represent the virtual levels (reprinted with permission from [44]).

APD was demonstrated in several experiments [43]; however the weak $\chi^{(2)}$ nonlinear interaction, a third-order process in the perturbation theory as explained in the introduction (figure 10(*a*)), limits the efficiency of this technique and the need for phasematching limits integration into semiconductor circuits.

Unlike insulating nonlinear crystals, semiconductors enable charge carrier transport, such that more efficient resonant low-order nonlinear processes can be used, taking advantage of generation and recombination of electrons and holes without the need for phasematching, thus allowing the realization of miniature devices in integrated photonic circuits. A simple scheme was proposed for IR single-photon direct detection in a Si APD assisted by a TPA process [44] at room temperature. In this scheme, the energy of the detected photon at the signal frequency $\omega_s$ is lower than the bandgap and the energy difference is complemented by a pump field at $\omega_p$. The pump frequency $\omega_p$ is sufficiently low to prevent TPA and three-photon absorption of the pump photons alone in Si. The proposed TPA-based detection (figure 10(*b*)) is a second-order resonant process, and therefore it is more efficient than the fourth-order up-conversion scheme.

The Si-based waveguide APD efficiency was calculated using the described model for practical device dimensions (∼1 mm length) [45]. The optimal pump power for the device was estimated to be around 1 kW, which is feasible with commercial ultrafast lasers.

However, experimental realizations of TPA-based IR photon detection in a Si APD appear to be difficult due to parasitic linear detection. The exact origin of the linear detection of photons with energy below the bandgap in a Si APD is not clear. A TPA-based IR photon detector was recently implemented in a GaAs PMT that does not suffer from residual one-photon absorption [46]. In this scheme, signal photons at 1.55 $\mu$m are detected in a GaAs photocounting module, assisted by an auxiliary laser at 1.9 $\mu$m (figure 11). The beams are combined on a beam splitter and a thick Si wafer is used to filter out any photons at wavelengths shorter than 900 nm to prevent one-photon absorption in the PMT. The beams are then focused on a GaAs PMT (H7421-50 Hamamatsu) that has a low DC rate of ∼40 counts $s^{-1}$.

The dependence of the TPA on the signal power was linear, as expected (figure 12(*a*)). Furthermore, the dependence of the TPA count rate on the signal wavelength was smooth (figure 12(*a*) inset) validating the fact that no

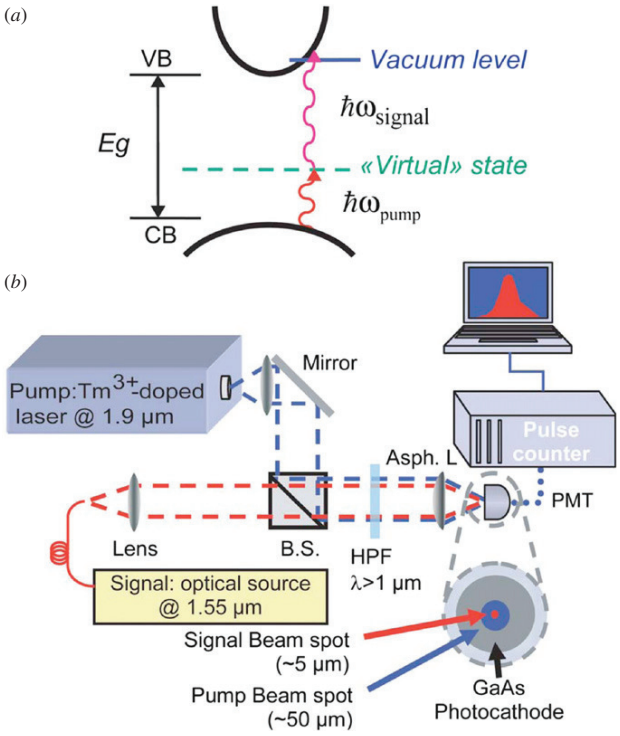


**Figure 11.** (*a*) IR quantum counting by TPA. (*b*) Experimental setup: two nearly collimated beams are combined using a beam splitter. Parasitic high energy photons are filtered out by a high pass filter. Beams are focused through an aspheric lens on a GaAs photocathode. The pump beam area on the GaAs detector is chosen far larger than the signal one in order to minimize nonlinear absorption effects due to the pump beam and to stabilize the overlap between the two beams against vibrations (reprinted with permission from [46]).

phasematching is required for TPA-based detection. The TPA efficiency measurements for different pump and signal powers (figure 12(*b*)) resulted in a TPA quantum efficiency of around $2 \times 10^{-3}$ $cm^4$ $W^{-2}$ for a pump power of up to $3.5 \times 10^3$ W $cm^{-2}$, which however decreased at higher pump powers, probably due to heating effects. The efficiency of the scheme can be further enhanced by waveguide geometries.

## 5. Coherent control with semiconductor TPA

The concept of coherent control relies on manipulation of an object by two or more phase-related excitations. The manipulated object may be a chemical reaction, atomic population, current flow and more, while the excitation is in many cases electromagnetic radiation. In this section we focus on coherent control processes which involve two-photon transition amplitudes in semiconductors.

Coherently controlled photocurrents in semiconductors were demonstrated in an experiment [47] where one- and two-photon absorption pathways were shown to interfere constructively at preferable crystal momentum, resulting in nonzero average photocurrent flow. In this process the two frequencies have to be phase related, i.e. created from the same laser source by frequency doubling. In this particular

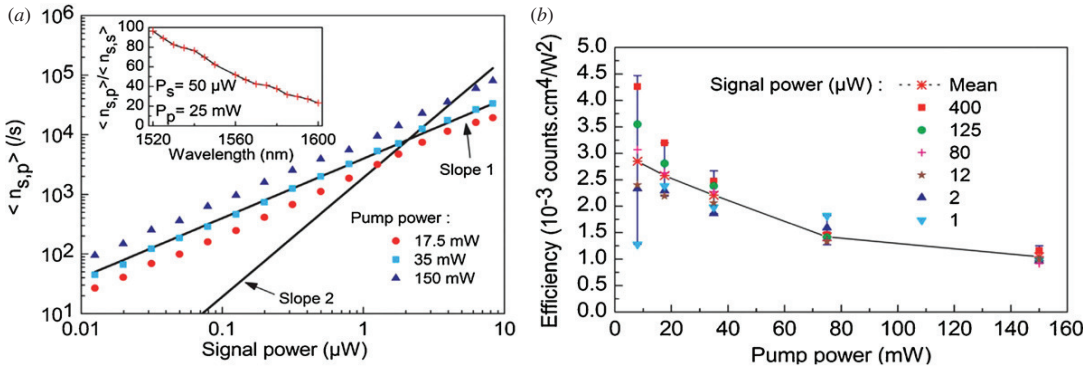


**Figure 12.** (*a*) TPA photocounts $\langle n_{s,p}\rangle$ as a function of the signal power for different pump intensities. The two solid lines represent a linear (slope 1) and a quadratic (slope 2) evolution profile. The inset displays the ratio $\langle n_{s,p}\rangle/\langle n_{s,s}\rangle$ at fixed pump and signal power for different signal wavelengths. (*b*) TPA-normalized efficiency for different pump and signal intensities (reprinted with permission from [46]).

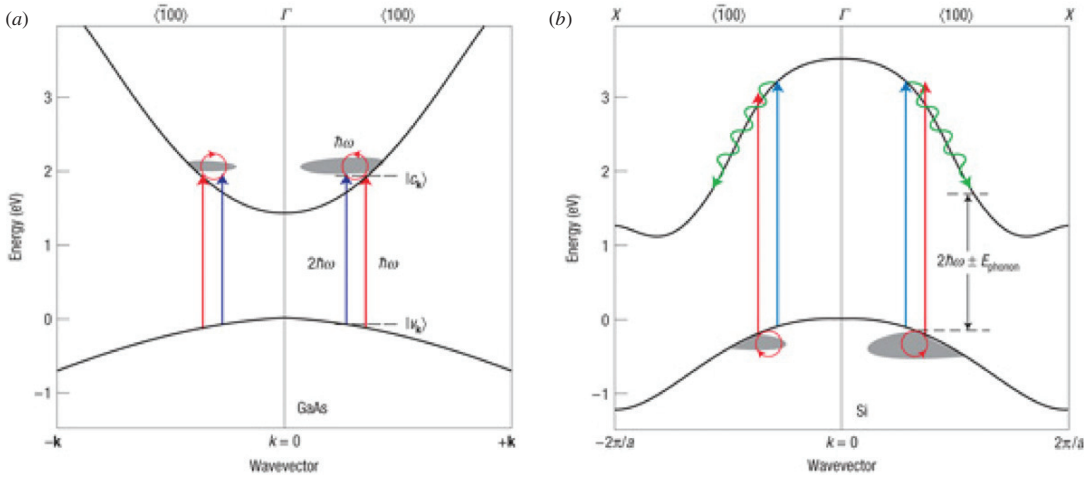


**Figure 13.** (*a*) Schematic energy–momentum band diagram of GaAs near the Γ point showing one conduction and one valence band and two-color excitation and interference across the fundamental bandgap; red is associated with the $\omega$ beam, blue with the $2\omega$ beam. Asymmetric electron populations at $\pm k$, and hence current generation is indicated by shaded patches. (*b*) Corresponding band diagram for Si along the Γ–*X* direction, showing interference for similar types of phonon-assisted transitions; phonon scattering with emission or absorption at the energy $E_{\text{phonon}}$ is indicated (reprinted with permission from [50]).

experiment the bound state of a GaAs 5.5 nm wide QW in a super-lattice structure (at a temperature of 82 K) was connected to the unbound continuum by a 5.3 $\mu$m laser and its second harmonic, operating in a ns pulsed regime. It was shown that the photocurrent detection depends on the relative phase between the first and second harmonics.

The theory for interband transition in a bulk structure was developed in [48]. Since in bulk crystals the continuum states have no determined parity, initial (valence band (VB)) and final (conduction band (CB)) states may be connected by one- as well as by two-photon transitions, opening the possibility for interference effects. The matrix elements of corresponding transitions are proportional to

$$\begin{aligned} a_{1-\text{photon}} &\sim \vec{p}_{cv}, \\ a_{2-\text{photon}} &\sim \vec{k}\cdot\vec{p}_{cv}, \end{aligned} \tag{8}$$

where $\vec{p}_{cv}$ is the electron momentum operator and $\vec{k}$ is the electron crystal momentum. The two-photon term may be evaluated by the second-order perturbation theory (equations (5) and (6)), relying on the summation over all possible intermediate states. In semiconductors, the most significant contributors to the summation are the initial and final states themselves, due to their undefined parity, resulting in the crystal momentum-dependent term (equation (8)). Properly designed pulses with a certain intensity and relative phase may cause constructive interference for preferable crystal momentum, resulting in a macroscopic current, dependent on the relative phase between the one- and two-photon excitations (figure 13(*a*)).

One year after the theoretical proposition, the successful measurement of the corresponding effect was reported [49]. Because of fast carrier's relaxation (100 fs) in room-temperature semiconductors and high intensities required for TPA, such experiments should be performed by fs pulses for macroscopic currents to be observed.

Another exciting effect occurs in indirect bandgap semiconductors, which may generate currents of similar

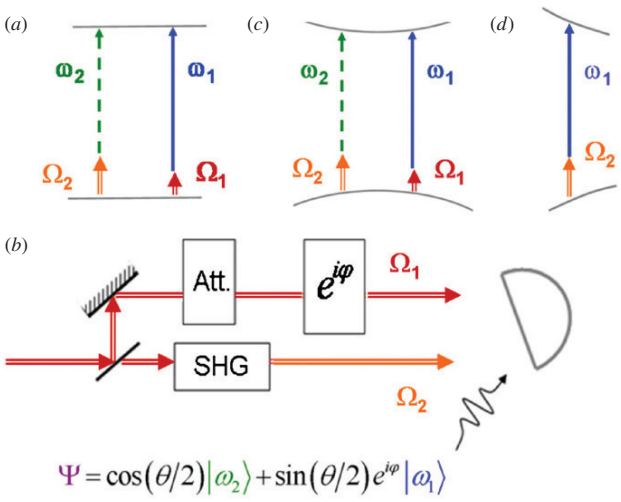


**Figure 14.** Direct characterization of energy entanglement. (*a*) Transition amplitude interference in TPA, (*b*) TPA interferometer realization scheme (*c*) semiconductor TPA interferometer implementation, (*d*) a parasitic TPA process of cross-coupling possible in semiconductors at high electron crystal momentum (reprinted with permission from [54]).

origin, involving additional phonon scattering [50] (figure 13(*b*)).

Furthermore, injection of spin currents in high-purity semiconductors even with complete crystal symmetry was proposed [51] and demonstrated [52], opening variety of additional applications. Coherent control of THz radiation from electron beating in an asymmetric double QW structure, excited by a sub-ps laser pulse and its second harmonic, was also proposed [53].

Recently, increasing interest in quantum information applications led to a proposed interference between two TPA paths to detect energy qubits and perform full Bell-state analysis [54]. This investigation together with the opposite process of semiconductor TPE (or down-conversion) opens new possibilities for semiconductor room-temperature integrable quantum communication technologies [55].

The proposed interferometry is performed by electron transition amplitudes in a TPA interferometer. Two auxiliary and mutually phase-locked lasers with frequencies $\Omega_1$ and $\Omega_2$, satisfying certain requirements, are used for two interfering paths of TPA, detecting the energy qubit state (figure 14).

Despite the different energy components in the detected photon at $\omega_1$ and $\omega_2$, the transition energies for each path are complemented by the auxiliary frequencies $\Omega_1 + \omega_1 = \Omega_2 + \omega_2$, allowing transition amplitude interference. Constructive interference will result in a detection event with high probability, whereas destructive interference will not result in detection.

## 6. Spontaneous TPE for quantum information

### *6.1. Semiconductor TPE process*

In TPE electron transitions between energy levels occur by simultaneous emission of a photon pair (figure 1(*a*)). TPA in semiconductors has been substantially studied in the last few decades; however semiconductor TPE has only recently been demonstrated [56]. First TPE experiments were performed on optically pumped GaAs with a very broad TPE spectrum according to the theory. Any possibility of inhomogeneously broadened one-photon emission from mid-gap levels was dismissed by singly stimulated TPE measurement (figure 1(*b*)), carried out by an additional tunable laser stimulating a specific wavelength in TPE and a complementary one, while the rest of the spontaneous emission spectrum was suppressed indicating homogeneous broadening due to very short lifetime of the virtual state (figure 15). The width of complementary peak is related to the carrier energy distribution (figure 15, inset).

TPE was then demonstrated in electrically pumped semiconductor devices consisting of 50 Å $Ga_{0.45}In_{0.55}P$ QWs separated by 55 Å $(Al_{0.5}Ga_{0.5})_{0.51}In_{0.49}P$ barriers, ∼1.1 $\mu$m AlGaInP cladding. The structure was electrically pumped below the lasing threshold, which was raised to above 200 mA by applying an anti-reflection coating on the facets, in order to enable higher carrier population inversion. The measured TPE power was around 30 nW—nearly five orders of magnitude weaker than the one-photon emission. Singly stimulated TPE was also demonstrated in electrically pumped GaInP/AlGaInP QWs; however, the effect of stimulation is much smaller in QWs than in bulk GaAs due to the very small overlap of the optical mode with the QWs ($<10^{-2}$). Photon coincidences were demonstrated in TPE from GaInP/AlGaInP QWs. The coincidence measurement is more difficult relative to other sources due to the low photon energies. For GaInP/AlGaInP QW TPE one Si APD was used along with one InGaAs APD, operated in gated mode at about 100 kHz repetition rate, resulting in nearly 10% coincidences determined by the losses.

Theoretical modeling of TPE in semiconductors has only recently begun, and solutions have been developed for special cases; however a full quantum theory of TPE in solids is still an open problem. The fundamental difference between two-photon processes in semiconductors and in atomic systems is the delocalized electron wavefunctions in solids with definite crystal momentum in contrast to the localized atomic states. The semiconductor's spontaneous TPE spectrum can be calculated similar to the atomic calculation scenarios [57] by a second-order time-dependent perturbation term with the $H = -\frac{e}{m_0}\vec{A}\cdot\vec{p}$ Hamiltonian in the dipole approximation, where $\vec{p}$ is the momentum operator, $e$ is the electron charge, $m_0$ is the free space electron mass and $\vec{A}$ is the vector potential operator. The most significant contribution to the second-order perturbation is made by the final and the initial states, included as the intermediate states with zero energy-separation from either initial or final state, and the resulting TPE rate is proportional to

$$M^2(\omega_1, E_{21}) \propto \left|\frac{1}{\mathrm{i}\omega_1 + \Gamma} + \frac{1}{\mathrm{i}\,(E_{21}/\hbar - \omega_1) + \Gamma}\right|^2 \times \omega_1\,(E_{21}/\hbar - \omega_1)\,, \tag{9}$$

where $E_{21}$ is the carrier energy separation, $\omega_1$ is the photon radial frequency and $\Gamma$ is a transition dephasing. In spontaneous TPE calculations, in the absence of the dephasing

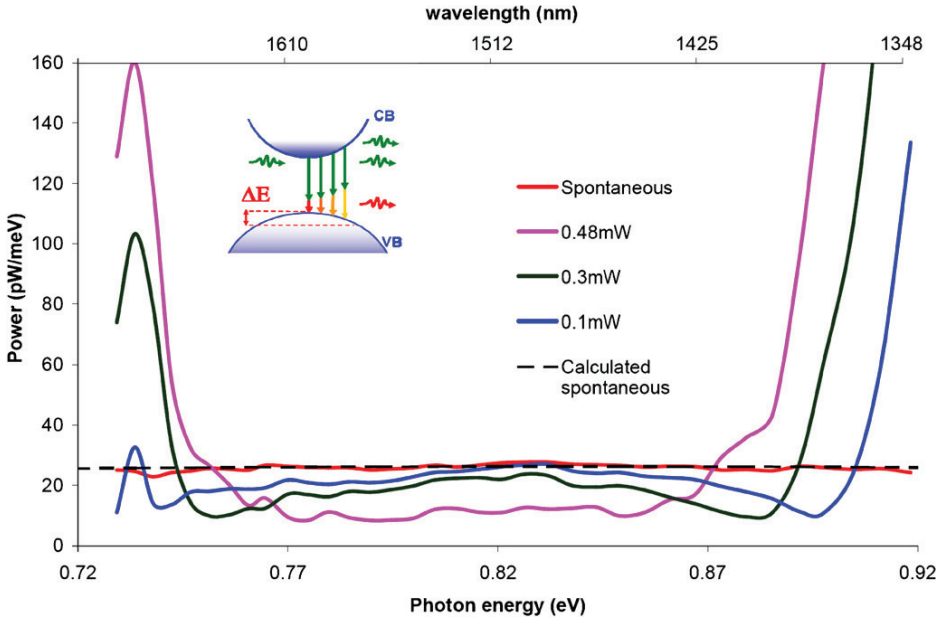


**Figure 15.** Bulk GaAs TPE measurements and calculations with optical pumping by a 180 mW, 514 nm Ar laser: spontaneous and singly stimulated TPE with various stimulation powers at 1310 nm. The inset is a schematic description of singly stimulated TPE energy broadening in bulk semiconductor (reprinted with permission from [56]).

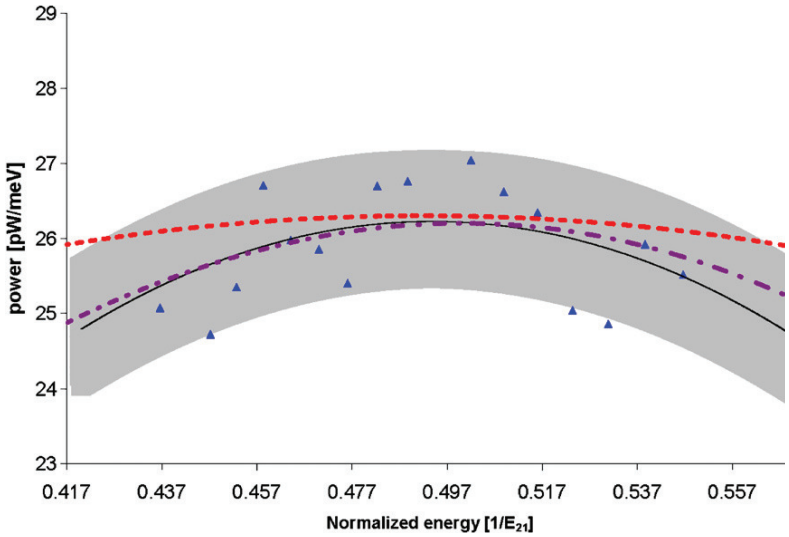


**Figure 16.** TPE spectrum versus energy normalized by the average carrier energy. Experimental measurements are marked by the blue triangles, the solid line (black) is the experimental quadratic fit, while the one-sigma variance is denoted by the grayed area; also shown are the calculated spectrum by the dressed state method with constant carrier dephasing time of <100 fs (dashed red) and calculated spectrum with the frequency-dependent carrier dephasing (dash-dot purple) (reprinted with permission from [59]).

term $\Gamma$, the matrix element divergence for $\omega_1 \rightarrow 0$ or $(E_{21}/\hbar - \omega_1) \rightarrow 0$ (equation (9)) causes an IR catastrophe and significantly distorts the spectrum shape.

An alternative semiclassical model to the second-order perturbation was developed recently using the dressed Volkov-state approach that eliminates the zero-energy divergence [58]. However, without the dephasing term the calculated spectrum remains distorted. In the developed dressed state approach one of the interacting fields dresses the initial and final electronic states of the semiconductor, represented as Volkov states [59] $\Psi(\vec{r}, t) = u(\vec{k}, \vec{r}) \exp i\vec{k}(\vec{r} + \delta\vec{r})$, where $u(\vec{k}, \vec{r})$ is the Bloch function, and the envelope phase is modulated by the classical trajectory of the electron oscillations with a mean dephasing time. The dephasing times in the conduction and valence bands are photon frequency dependent—determined by carrier–carrier scattering rates including the temporal dependence of the screening build-up. This dephasing frequency dependence yields a significant correction to the TPE spectrum shape, conforming to experimental results (figure 16).

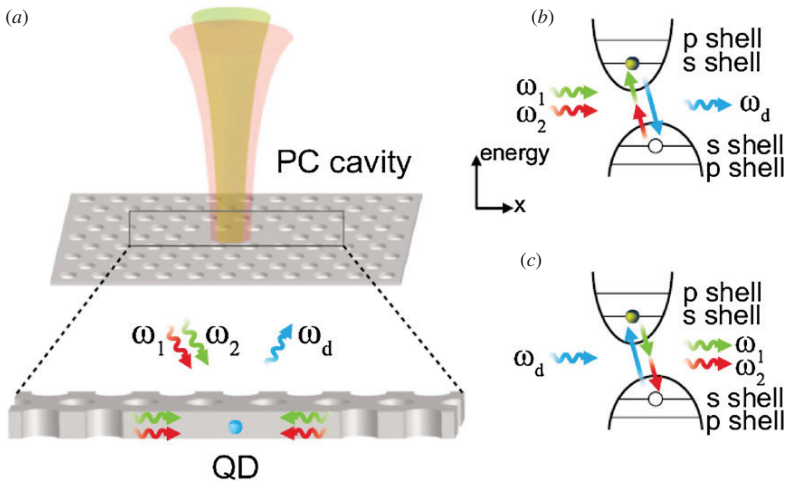


**Figure 17.** (*a*) Setup for the enhanced TPA experiment: two laser beams with frequencies $\omega_1$ and $\omega_2$ are injected into a double-mode cavity. (*b*) Enhanced TPA and single-photon generation in a QD with a lateral electric field applied to it in the lateral *X* direction. The lateral electric field shifts apart the hole VB and the electron CB and therefore breaks the parity selection rule. (*c*) Enhanced two-photon spontaneous emission in a QD as a reverse process of TPA. The one-photon-excited electron recombines with the hole and generates entangled photon pair via two-photon spontaneous emission (reprinted with permission from [60]).

### *6.2. Enhancement of TPE by nanocavities*

TPE, being a nonlinear emission process, is relatively weak, and can significantly benefit from various enhancement mechanisms.

Enhancement of TPE from QDs was proposed by coupling the emission to photonic crystal nanocavities, which also enhances coherent excitation of the QDs by TPA [60]. A theoretical model was developed for enhancement of TPA, spontaneous TPE and stimulated TPE from a single QD in a nanocavity (figure 17). A special cavity was designed to achieve degenerate TPA at ultralow powers of $\sim$10 $\mu$W, enabling coherent excitation of QDs by TPA and on-demand generation of photon pairs by TPE with enhancement of several orders of magnitude relative to the emission without cavities. Another design was developed for the non-degenerate TPE case which can be used to generate single photons.

Dielectric optical microcavities with a high quality factor ($Q$) enhance specific-wavelength emission; however they are less suitable for the broad spectrum of TPE. Plasmonic nanostructures allow reducing the modal volume for local field enhancement, however retaining a low $Q$, which is optimal for TPE. An experimental observation of semiconductor's spontaneous TPE enhanced by coupling to bow-tie nanoantenna arrays (figures 18(*a*) and (*b*)) was recently reported [61]. AlGaAs TPE spectrum reshaping was demonstrated (figure 18(*c*)) and the enhancement was verified to decrease with spectral detuning of the antenna resonance from the TPE center. A thin AlGaAs layer was grown on the GaAs substrate, separated by a wider bandgap AlGaAs for the confinement of the charge carriers to the near-field of the nanoantennas, and the emission was verified to be TPE by singly stimulated emission experiments.

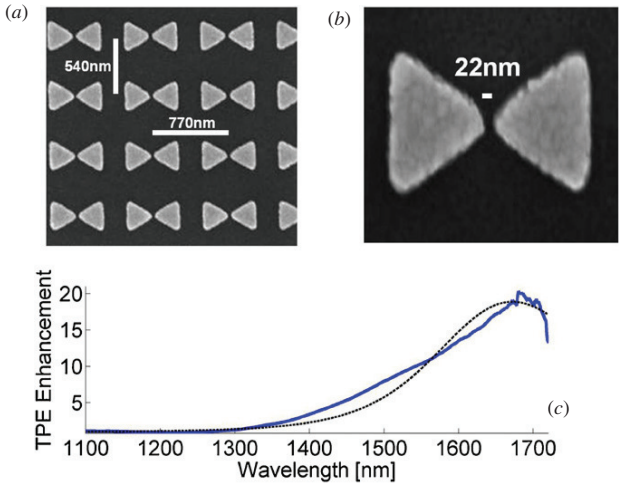


**Figure 18.** (*a*), (*b*) SEM image of the particles at two different magnifications. (*c*) Spectrum of the enhancement in TPE by the bow-tie array: measurement—the solid blue line, FDTD calculation—the dashed black line (reprinted with permission from [61]).

### *6.3. Entanglement sources by TPE in semiconductors*

Entanglement is an essential resource for realizing many quantum information protocols, such as teleportation and quantum networking. All-optical quantum computing schemes would also greatly benefit from an on-demand source of entangled photons.

Although compact semiconductor sources of entangled photons have been realized, using QD emission, they operate at cryogenic temperatures. The most widely used room-temperature source of entangled photons today is PDC based on crystals with a $\chi^{(2)}$ nonlinearity. The main efficiency limitation of PDC-based entanglement sources is the weak

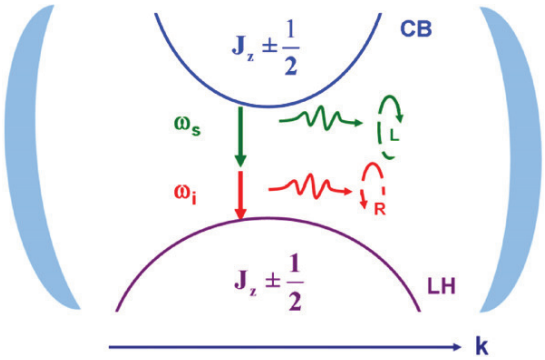


**Figure 19.** Cavity-controlled TPE entanglement source (reprinted with permission from [62]).

fundamental interaction, described by a third-order non-resonant process in the time-dependent perturbation theory combined with a first-order process of the pump laser emission with ~10% efficiency. The probability of PDC is proportional to $\alpha^3$, where $\alpha$ is the fine-structure constant.

A highly efficient room-temperature source of entangled photons was proposed based on QW TPE in a microcavity [62]. The probability of TPE is calculated via the second-order term in the perturbation theory and is therefore proportional to $\alpha^2$, and is expected to be stronger than PDC by at least $10/\alpha \sim 10^3$ for equal pump levels. In the proposed scheme the device is electrically driven, and a doubly resonant microcavity is designed to select the two-photon transition wavelength modes: the signal $\omega_s$ and the idler $\omega_i$. In an ideal TPE-based source where one-photon emission is suppressed, majority of carriers will recombine to emit a photon pair—similar to optically pumped PDC with conversion efficiency near unity. However, in realistic electrically pumped semiconductor devices, the non-radiative recombination is the dominant process and it determines the carrier density and the TPE rate, regardless of the residual one-photon emission rate.

For certain strained QWs, the light hole band may have the highest energy, so that the angular momentum in the direction of the QW growth ($z$) in the VB is $j_z = \pm 1/2$ and in the CB is $j_z = \pm 1/2$, and transitions between states of definite angular momentum will result in net angular momentum change of $\Delta j_z = \pm 1$ or $\Delta j_z = 0$. Therefore TPE-related transitions have total angular momentum change of $\Delta j_z = 0$. The cavity is designed to have high top mirror reflectivity and the photon pairs emitted will therefore have opposite polarizations and can be separated by a polarization beam splitter. In TPE energy conservation $\hbar(\omega_i + \omega_s) = E_{\mathrm{CB}} - E_{\mathrm{VB}}$ does not determine the energy of each individual photon and the emitted two-photon state is therefore energy-entangled. The wavefunction of the emitted photon pair is

$$|\Psi\rangle = \frac{1}{\sqrt{2}} \left( |\omega_i\rangle_R \, |\omega_s\rangle_L + |\omega_s\rangle_R \, |\omega_i\rangle_L \right), \tag{10}$$

where the entangled particles are identified by the circular polarization (right or left) (figure 19).

The microcavity enhances the emission at the desired wavelengths and suppresses the rest of the spectrum. The TPE-based photon pair generation rate in the structure was calculated to be around tens of GHz—nearly three orders of magnitude higher than those of the PDC-based sources.

Intersubband transitions in QWs were proposed for hyperentangled photon sources—entangled in both energy and polarization [63]. Selection rules for some of the QW intersubband TPE transitions determine the in-plane emitted photons to be polarized orthogonally, however without determining the polarization of each individual photon.

Furthermore, the energies of the two emitted photons must sum up to the energy level separation, while each photon's energy is not determined. Therefore the photon pairs will be hyperentangled in both energy and polarization (figure 20), so that the general hyperentangled state of the emitted pairs is

$$\psi = \int g(\omega)[|\omega, \varepsilon_z\rangle_1 |\omega_{if} - \omega, \varepsilon_\perp\rangle_2 + |\omega, \varepsilon_\perp\rangle_1 |\omega_{if} - \omega, \varepsilon_z\rangle_2] \, \mathrm{d}\omega, \tag{11}$$

These TPE-based hyperentanglement sources should have pair generation rates several orders of magnitude higher than those of the alternative schemes.

## 7. TPG in semiconductor devices

Two-photon stimulated emission, the process in which two photons with sum-energy equal to the energy gap stimulate an

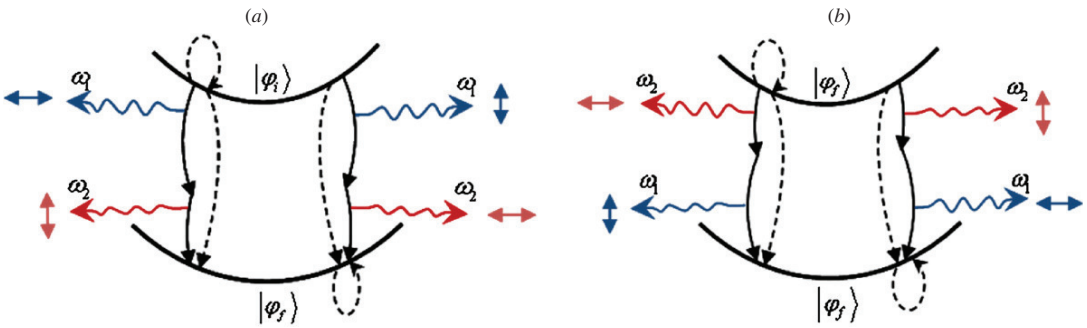


**Figure 20.** Schematic description of QW intersubband TPE with orthogonal polarizations. The solid arrows are the electronic transitions via virtual states, while the dashed arrows represent the matrix element calculations via intermediate states. (*a*), (*b*) Symmetrical Feynman diagrams with interchanged vertices (reprinted with permission from [63]).

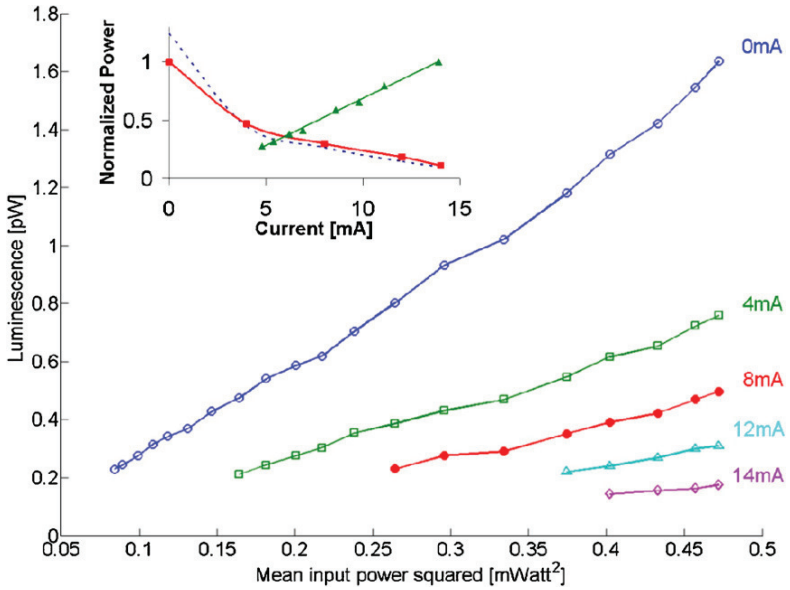


**Figure 21.** Measured electrically controlled TPA luminescence versus input power squared at various currents. No current (blue circles), 4 mA (green squares), 8 mA (red filled circles), 12 mA (cyan triangles) and 14 mA (purple diamonds) (reprinted with permission from [71]).

electron transition resulting in their duplication (figure 1(*c*)), was proposed soon after the invention of the laser [64]. It was identified that, due to the inherent nonlinearity of the process (higher intensities are amplified stronger), two-photon amplifiers and lasers will exhibit unique classical behavior including bi-stability and giant pulse generation [65] as well as quantum properties such as squeezing [66]. A decade after the observation of singly stimulated TPE [67], fully stimulated TPE was observed [68] leading to the demonstration of a two-photon laser (TPL) [69], where all experiments were performed on discrete-level atomic systems. The main drawback of these schemes was their complexity, arising from the fact that strong optical pumping results in competing nonlinear effects such as self-focusing, stimulated anti-stokes Raman scattering and parametric wave mixing. Moreover, the atomic TPLs provided relatively low powers, primarily due to the small numbers of interacting atoms.

Since semiconductors have orders of magnitude higher carrier concentrations in respect to atomic systems, and since they can be electrically pumped, it was suggested that semiconductor-based two-photon amplifiers can provide a compact high-power alternative to the atomic configurations [70]. The analysis focused on the degenerate case in which photons with energy below the energy gap are duplicated in pairs, usually regarded as degenerate TPG. Although semiconductor TPA has been substantially investigated and is widely employed, as demonstrated in this review, the opposite process of TPG in semiconductors was only recently observed.

In a degenerate TPG medium, the spatial dependence on the light intensity, $I$, propagating in the $z$ direction, neglecting higher order nonlinearities, is given by

$$\mathrm{d}I/\mathrm{d}z = \Gamma\gamma_2' I^2 - \alpha I, \tag{12}$$

where $\Gamma$ is the confinement factor of the waveguide, $\alpha$ is the linear loss coefficient and $\gamma_2'$ is the semiconductor TPG coefficient given by

$$\gamma_2' = \frac{8\pi\omega_s}{I^2}\sum_f \int \frac{\mathrm{d}^3k}{(2\pi)^3}(F_c(k) - F_v(k)) \times \left|\sum_n \frac{\langle f|\,H\,|n\rangle\langle n|\,H\,|i\rangle}{E_n - E_i - \hbar\omega_s}\right|^2. \tag{13}$$

Here $F_c(k)$ and $F_v(k)$ are the quasi Fermi–Dirac distribution functions in the conduction and valence bands respectively, and indices $f$, $n$ and $i$ stand for the final, intermediate and initial states accordingly, while energy conservation dictates $E_f - E_i = 2\hbar\omega_s$.

It is important to note that $\gamma_2'$ is current dependent due to the injection-induced change in the separation of the quasi Fermi levels $E_{FC}$ and $E_{FV}$ of the conduction and valence bands respectively (equation (13)). When the separation satisfies the two-photon population inversion condition $E_{FC} - E_{FV} > 2\hbar\omega_s$, $\gamma_2'$ becomes positive resulting in TPG, while at lower carrier injection the gain is negative, corresponding to TPA. $\alpha$ depends on the charge carrier concentration mainly due to free carrier absorption (FCA). It was first shown experimentally that standard semiconductor laser structures based on multiple quantum wells (MQWs) may exhibit two-photon transparency (TPT) under current injection [71], meaning that the TPA rate is reduced with current injection (figure 21) until reaching the transparency point for which the probabilities for TPA and for TPG are equal. The experiments suggested that the QW structure is less suitable for efficient TPG due to the very small confinement of the optical mode to the active region, as was also predicted in [72]. In order to track the relatively weak nonlinear changes of strong pulses propagating in the semiconductor waveguide, an indirect method was employed; changes in two-photon-induced luminescence controlled by an electrical current in an AlGaAs MQW

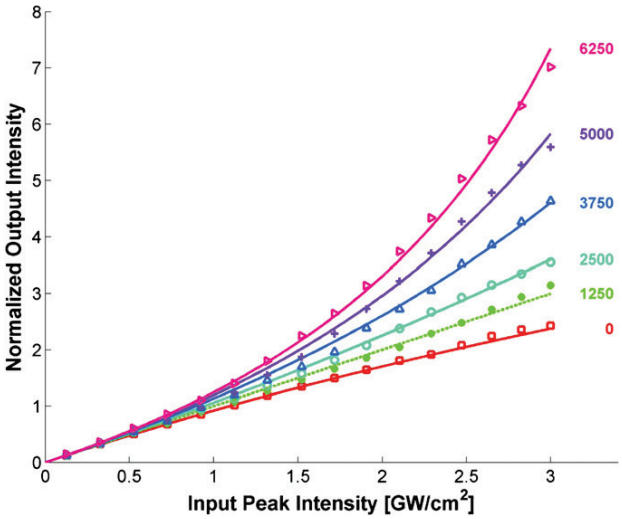


**Figure 22.** Direct measurements of 1560 nm TPG for a 2.9 mm long waveguide at different current densities (in units of A cm$^{-2}$ $\mu$m$^{-1}$) normalized by the linear slope coefficient of each graph at low input powers (reprinted with permission from [73]).

structure were monitored in a lock-in detection scheme, in which pulses with central wavelength of 1.56 $\mu$m are chopped and changes in luminescence at the chopping frequency are detected.

In order to reach TPG and observe it directly, a bulk structure was designed, having an order of magnitude higher confinement factor in respect to the MQW device [73]. The highly nonlinear behavior of the output intensity in respect to the input intensity at 1.56 $\mu$m was examined. The solution of equation (12) for a device length $L$ with an input intensity $I_0$ is

$$I_{\text{out}} = I_0 e^{-\alpha L}/[1 - \gamma_2 I_0(1 - e^{-\alpha L})/\alpha]. \quad (14)$$

Therefore, the output intensity exhibits concave dependence on input intensity for TPA ($\gamma_2 < 0$) (higher intensity is absorbed stronger), linear dependence on input intensity for TPT ($\gamma_2 = 0$), and convex dependence on input intensity for TPG ($\gamma_2 > 0$) (higher intensity is amplified stronger). TPA, TPT and TPG measurements at various current densities (figure 22) yielded for the device length of 2.9 mm a $\gamma_2$ value of 3.15 cm GW$^{-1}$ at a charge carrier concentration of $\sim 3 \times 10^{18}$ cm$^{-3}$ and a linear loss of $\alpha = 15.8$ cm$^{-1}$.

TPG was proposed as a promising candidate for ultrashort pulse generation [74] based on the fact that the high-intensity peak of a short pulse propagating in a TPG medium is amplified stronger than the low-intensity tails—resulting in pulse compression. It was shown numerically that since TPG has an extremely wideband homogeneous spectrum, pulses may be compressed down to a few optical cycles [75]. It is interesting to note that since the amplification term is nonlinear, pulse compression may be achieved even without net gain—in the presence of strong linear losses. Recently, an experimental demonstration of pulse compression in a TPG amplifier was presented [28]. TPG-induced pulse compression of nearly 40% compared to the original output pulse was measured for an input pulse of ~170 fs using 1 mm long AlGaAs waveguides, controlled continuously by electrical pumping (figure 23). The pulse width measurements were based on a collinear intensity autocorrelation setup based on TPA in a GaAs PMT (figure 5).

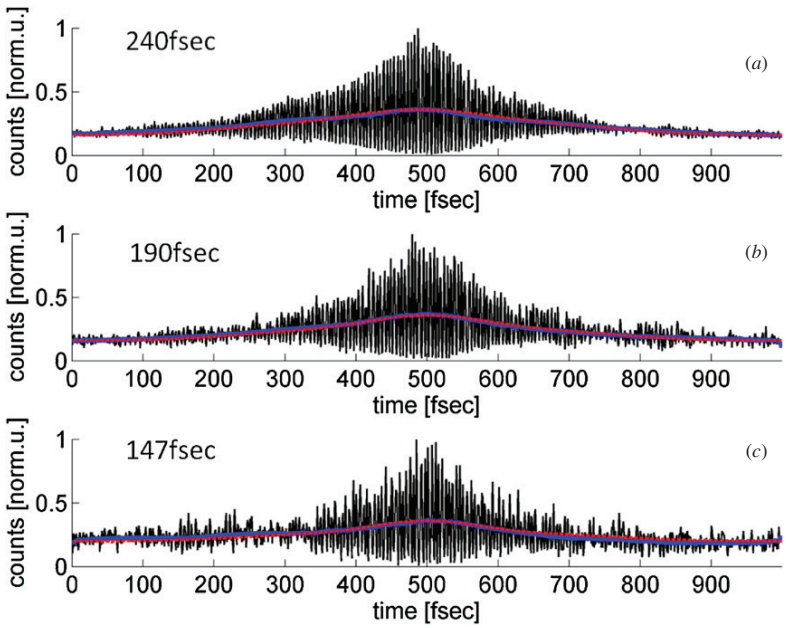


**Figure 23.** PMT photocounts (normalized by the counts at the autocorrelation peak) as a function of the delay $\tau$ in the Michelson setup for the 1.56 $\mu$m central wavelength pulse, after propagating 1 mm in the waveguide with (*a*) no current injection, (*b*) current density of 1200 A cm$^{-2}$ $\mu$m$^{-1}$, (*c*) current density of 2800 A cm$^{-2}$ $\mu$m$^{-1}$ (reprinted with permission from [28]).

The pulse compression measurement demonstrates the great potential of semiconductor TPG for applications in ultrafast integrated photonics. The next expected step in research will be to achieve two-photon lasing in a miniature semiconductor device. TPLs require a seed pulse, since the spontaneous TPE is not strong enough to bring the TPG values to overcome the losses. A simplified condition can be deduced from equation (12) for self-maintained oscillations inside the waveguide which is $\Gamma\gamma_2' I > \alpha_{\text{int}} + \alpha_m$ where $\alpha_m$ stands for mirror loss at each round trip, and the nonlinear amplification is of course limited by saturation, such that $\gamma_2' = \gamma_{2,0}'/\left(1 + \frac{I^2}{I_0^2}\right)$. Intersubband transitions in QWs were suggested for achieving strong TPG coefficient and lasing [76], and using QDs in high-$Q$ microcavities to achieve enough intensity was proposed for two-photon lasing [77].

## 8. Summary and outlook

We have shown that two-photon processes in semiconductors, often regarded as weak and impractical, may serve efficiently for various applications. The unique characteristics of the two-photon process make it superior in respect to other room-temperature schemes based on all-optical nonlinear processes. Ultrafast optical multiplication based on TPA is becoming a dominant tool for autocorrelation, either for classical measurements of pulse widths as well as for unique quantum measurements, which could not have been achieved by electronic multiplication. Signal processing and logic by TPA may become more significant as the design of integrated cavities in which the process is highly efficient will continue to improve. The ultrashort pulse compression by semiconductor TPG may enable generating ultrafast pulses close to the sample they act on in medical applications, or miniature components for dispersion compensation in communication applications. It should be noted that semiconductor TPA may sometimes be an undesirable and limiting process, e.g. for efficient Raman amplification in silicon [78], where TPA induces FCA. Quantum applications based on coherent control, single-photon and entangled-photon sources, as well as quantum logic, presented in this review may serve as building blocks for the future design of integrated quantum technologies. Other techniques based on cascaded one-photon emission, e.g. from biexcitons [79] in QDs, were not covered in this review. A foreseen next step in the field of semiconductor two-photon processes may involve the realization of a semiconductor TPL, novel nanocavity implementation for TPE enhancement and enhanced collection efficiency for quantum sources, as well as integration of quantum detectors based on two-photon processes on a chip.

## References


[1] Maier M, Kaiser W and Giordmaine J A 1966 Intense light bursts in the stimulated Raman effect *Phys. Rev. Lett.* **17** 1275–7

[2] Armstrong J A 1967 Measurement of picosecond laser pulse widths *Appl. Phys. Lett.* **10** 16

[3] Mogi K, Naganuma K and Yamada H 1988 A novel real-time chirp measurement method for ultrashort optical pulse *Japan. J. Appl. Phys.* **27** 2078–81

[4] Weber H P 1967 Method for pulsewidth measurement of ultrashort light pulses generated by phase locked lasers using nonlinear optics *J. Appl. Phys.* **38** 2231–4

[5] Takagi Y, Kobayashi T, Yoshihara K and Imamura S 1992 Multiple- and single-shot autocorrelator based on two-photon conductivity in semiconductors *Opt. Lett.* **17** 658–60

[6] Salem R and Murphy T E 2004 Polarization-insensitive cross correlation using two-photon absorption in a silicon photodiode *Opt. Lett.* **29** 1524–6

[7] Laughton F R, Marsh J H, Barrow D A and Portnoi E L 1994 The two-photon absorption semiconductor waveguide autocorrelator *IEEE J. Quantum Electron.* **30** 838–45

[8] Skovgaard P M W, Mullane R J, Nikogosyan D N and McInerney J G 1998 Two-photon conductivity in semiconductor waveguide autocorrelators *Opt. Commun.* **153** 78–82

[9] Tsang H K, Chan L Y, Soole J B D, LeBlanc H P, Koza M A and Bhat R 1995 High sensitivity autocorrelation using two-photon absorption in InGaAsP waveguides *Electron. Lett.* **31** 1773–5

[10] Barry L P, Thomsen B C, Dudley J M and Harvey J D 1998 Autocorrelation and ultrafast optical thresholding at 1.5 $\mu$m using a commercial InGaAsP 1.3 $\mu$m laser diode *Electron. Lett.* **34** 358–60

[11] Liang T K, Tsang H K, Day I E, Drake J, Knights A P and Asghari M 2002 Silicon waveguide two-photon absorption detector at 1.5 $\mu$m wavelength for autocorrelation measurements *Appl. Phys. Lett.* **81** 1323

[12] Kikuchi K 1998 Highly sensitive interferometric autocorrelator using Si avalanche photodiode as two-photon absorber *Electron. Lett.* **34** 123–5

[13] Rudolph W, Sheik-Bahae M, Bernstein A and Lester L F 1997 Femtosecond autocorrelation measurements based on two-photon photoconductivity in ZnSe *Opt. Lett.* **22** 313–5

[14] Ranka J K, Gaeta A L, Baltuska A, Pshenichnikov M and Wiersma D 1997 Autocorrelation measurements of 6 fs pulses based on the two-photon-induced photocurrent in a GaAsP photodiode *Opt. Lett.* **17** 1344

[15] Krug T, Lynch M, Bradley A L, Donegan J F, Barry L P, Folliot H, Roberts J S and Hill G 2004 High-sensitivity two-photon absorption microcavity autocorrelator *IEEE Photon. Technol. Lett.* **16** 1543

[16] Reid D T, Sibbett W, Dudley J M, Barry L P, Thomsen B and Harvey J D 1998 Commercial semiconductor devices for two photon absorption autocorrelation of ultrashort light pulses *Appl. Opt.* **37** 8142–4

[17] Streltsov A M, Ranka J K and Gaeta A L 1998 Femtosecond ultraviolet autocorrelation measurements based on two-photon conductivity in fused silica *Opt. Lett.* **23** 798–800

[18] Zavriyev A, Dupont E, Corkum P B, Liu H C and Biglov Z 1995 Direct autocorrelation measurements of mid-infrared picosecond pulses by quantum-well devices *Opt. Lett.* **20** 1886

[19] Schneider H, Maier T, Liu H C, Walther M and Koidl P 2005 Ultrasensitive femtosecond two-photon detector with resonantly enhanced nonlinear absorption *Opt. Lett.* **30** 287–9

[20] Maier T, Schneider H, Walther M, Koidl P and Liu H C 2004 Resonant two-photon photoemission in quantum-well infrared photodetectors *Appl. Phys. Lett.* **84** 5162

[21] Schneider H, Drachenko O, Winnerl S, Helm M and Walther M 2006 Quadratic autocorrelation of free-electron laser radiation and photocurrent saturation in two-photon quantum well infrared photodetectors *Appl. Phys. Lett.* **89** 133508

[22] Schneider H, Maier T, Liu H C and Walther M 2008 Two-photon photocurrent autocorrelation using intersubband transitions at nearly-resonant excitation *Opt. Express* **16** 1523–8

[23] Collins D, Jarjour A, Hadjipanayi M, Taylor R, Oliver R, Kappers M, Humphreys C and Tahraoui A 2009 Two-photon autocorrelation measurements on a single InGaN/GaN quantum dot *Nanotechnology* **20** 245702

[24] Roth J M, Murphy T E and Xu C 2002 Ultrasensitive and high-dynamic-range two-photon absorption in a GaAs photomultiplier tube *Opt. Lett.* **27** 2076

[25] Barry L P, Bollond P G, Dudley J M, Harvey J D and Leonhardt R 1996 Autocorrelation of ultrashort pulses at 1.5 $\mu$m based on nonlinear response of silicon photodiodes *Electron. Lett.* **32** 1922

[26] Xu C, Roth J M, Knox W H and Bergman K 2002 Ultra-sensitive autocorrelation of 1.5 $\mu$m light with single photon counting silicon avalanche photodiode *Electron. Lett.* **38** 86

[27] Boitier F, Godard A, Rosencher E and Fabre C 2009 Measuring photon bunching at ultrashort timescale by two-photon absorption in semiconductors *Nat. Phys.* **5** 267

[28] Nevet A, Hayat A and Orenstein M 2010 Ultrafast pulse compression by semiconductor two-photon gain *Opt. Lett.* **35** 3877

[29] Steinmeyer G 2003 A review of ultrafast optics and optoelectronics *J. Opt.* A *Pure Appl. Opt.* **5** R1

[30] Cormack I G, Sibbett W and Reid D T 2001 Rapid measurement of ultrashort-pulse amplitude and phase from a two-photon absorption sonogram trace *J. Opt. Soc. Am.* B **18** 1377–82

[31] Thomsen B C, Barry L P, Dudley J M and Harvey J D 1998 Ultrahigh speed all-optical demultiplexing based on two-photon absorption in a laser diode *Electron. Lett.* **34** 1871

[32] Maguire P J, Barry L P, Krug T, Guo W H, O'Dowd J, Lynch M, Bradley A L, Donegan J F and Folliot H 2006 Optical signal processing via two-photon absorption in a semiconductor microcavity for the next generation of high-speed optical communications network *J. Lightwave Technol.* **24** 2683

[33] Zheng Z, Weiner A M, Marsh J H and Karkhanehchi M M 1997 Ultrafast optical thresholding based on two-photon absorption GaAs waveguide photodetectors *IEEE Photon. Technol. Lett.* **9** 493–5

[34] Saito T, Yano Y and Henmi N 1994 Optical TDM 20 Gb/s-105 km transmission [employing newly proposed optical PLL timing extraction *IEEE Photon. Technol. Lett.* **6** 555

[35] Awad E, Cho P S, Moulton N and Goldhar J 2003 Subharmonic optical clock recovery from 160 Gb/s using time-dependent loss saturation inside a single electroabsorption modulator *IEEE Photon. Technol. Lett.* **15** 1764

[36] Shumakher E, Hayat A, Freimain A, Nazarathy M and Eisenstein G 2004 Timing extraction of a 10-gb/s NRZ signal using an electro-optic multiplication scheme *IEEE Photon. Technol. Lett.* **16** 2353

[37] Salem R and Murphy T E 2004 Broad-band optical clock recovery system using two-photon absorption *IEEE Photon. Technol. Lett.* **16** 2141

[38] Salem R, Tudury G E, Horton T U, Carter G M and Murphy T E 2005 Polarization-insensitive optical clock recovery at 80 Gb/s using a silicon photodiode *IEEE Photon. Technol. Lett.* **17** 1968

[39] Liang T K, Nunes L R, Tsuchiya M, Abedin K S, Miyazaki T, Van Thourhout D, Bogaerts W, Dumon P, Baets R and Tsang H K 2006 High speed logic gate using two-photon absorption in silicon waveguides *Opt. Commun.* **265** 171

[40] Ibrahim T A, Grover R, Kuo L-C, Kanakaraju S, Calhoun L C and Ho P-T 2003 All-optical AND/NAND logic gates using semiconductor microresonators *IEEE Photon. Technol. Lett.* **15** 1422

[41] Xu Qi and Lipson M 2007 All-optical logic based on silicon micro-ring resonators *Opt. Express* **15** 924

[42] Ibrahim T A, Amarnath K, Kuo L C, Grover R, Van V and Ho P-T 2004 Photonic logic NOR gate based on two symmetric microring resonators *Opt. Lett.* **29** 2779

[43] VanDevender A P and Kwiat P G 2004 High efficiency single photon detection via frequency up-conversion *J. Mod. Opt.* **51** 1433

[44] Hayat A, Ginzburg P and Orenstein M 2008 Infrared single-photon detection by two-photon absorption in silicon *Phys. Rev.* B **77** 125219

[45] Pearsall T P, Temkin H, Bean J C and Luryi S 1986 Avalanche gain in $Ge_xSi_{1-x}$/Si infrared waveguide detectors *IEEE Electron Device Lett.* **7**

[46] Boitier F, Dherbecourt J-B, Godard A and Rosencher E 2009 Infrared quantum counting by nondegenerate two photon conductivity in GaAs *Appl. Phys. Lett.* **94** 081112

[47] Dupont E, Corkum P B, Liu H C, Buchanan M and Wasilewski Z R 1995 Phase-controlled currents in semiconductors *Phys. Rev. Lett.* **74** 3596–9

[48] Atanasov R, Haché A, Hughes J L P, van Driel H M and Sipe J E 1996 Coherent control of photocurrent generation in bulk semiconductors *Phys. Rev. Lett.* **76** 1703–6

[49] Haché A, Kostoulas Y, Atanasov R, Hughes J L P, Sipe J E and van Driel H M 1997 Observation of coherently controlled photocurrent in unbiased, bulk GaAs *Phys. Rev. Lett.* **78** 306–9

[50] Costa L, Betz M, Spasenovic M, Bristow A D and van Driel H M 2007 All-optical injection of ballistic electrical currents in unbiased silicon *Nat. Phys.* **3** 632–5

[51] Bhat R D R and Sipe J E 2000 Optically injected spin currents in semiconductors *Phys. Rev. Lett.* **85** 5432–5

[52] Stevens M J, Smirl A L, Bhat R D R, Sipe J E and van Driel H M 2002 Coherent control of an optically injected ballistic spin-polarized current in bulk GaAs *J. Appl. Phys.* **91** 4382

[53] Pötz W 1998 Coherent control of terahertz radiation from semiconductor nanostructures *Appl. Phys. Lett.* **72** 3002

[54] Hayat A, Ginzburg P and Orenstein M 2009 Photon energy entanglement characterization by electronic transition interference *Opt. Express* **17** 21280–8

[55] Ginzburg P, Shalyt M, Hayat A and Orenstein M 2010 Photon-energy qubit generation by spontaneous emission in a V-type system *J. Phys. B: At. Mol. Opt. Phys.* **43** 105502

[56] Hayat A, Ginzburg P and Orenstein M 2008 Observation of two-photon emission from semiconductors *Nat. Photon.* **2** 238

[57] Goppert-Mayer M 1931 Ueber Elementarakte mit zwei Quanenspruengen *Ann. Phys.* **9** 273–94

[58] Sheik-Bahae M, Hutchings D C, Hagan D J and Van Stryland E W 1991 Dispersion of bound electron nonlinear refraction in solids *IEEE J. Quantum Electron.* **27** 1296

[59] Hayat A, Ginzburg P and Orenstein M 2009 Measurement and model of the infrared two-photon emission spectrum of GaAs *Phys. Rev. Lett.* **103** 023601

[60] Lin Z and Vučković J 2010 Enhanced two-photon processes in single quantum dots inside photonic crystal nanocavities *Phys. Rev.* B **81** 035301

[61] Nevet A, Berkovitch N, Hayat A, Ginzburg P, Ginzach S, Sorias O and Orenstein M 2010 Plasmonic nano-antennas for broadband enhancement of two-photon emission from semiconductors *Nano Lett.* **10** 1848

[62] Hayat A, Ginzburg P and Orenstein M 2007 High-rate entanglement source via two-photon emission from semiconductor quantum wells *Phys. Rev.* B **76** 035339
[63] Hayat A, Ginzburg P, Neiman D, Rosenblum S and Orenstein M 2008 Hyperentanglement source by intersubband two-photon emission from semiconductor quantum wells *Opt. Lett.* **33** 1168
[64] Sorokin P P and Braslau N 1964 Some theoretical aspects of proposed double quantum stimulated emission device *IBM J. Res. Dev.* **8** 177
[65] Prokhorov A M 1965 Quantum electronics *Science* **149** 828
[66] Scully M O, Wodkiewicz K, Zubairy M S, Bergou J, Lu N and Meyer ter Vehn J 1988 Two-photon correlated–spontaneous-emission laser: quantum noise quenching and squeezing *Phys. Rev. Lett.* **60** 1832
[67] Yatsiv S, Rokni M and Barak S 1968 Enhanced two-photon emission *Phys. Rev. Lett.* **20** 1282
[68] Loy M M T 1978 Two-photon adiabatic inversion *Phys. Rev. Lett.* **41** 473
[69] Gauthier D J, Wu Q, Morin S E and Mossberg T W 1992 Realization of a continuous-wave, two-photon optical laser *Phys. Rev. Lett.* **68** 464
[70] Ironside C N 1992 Two-photon gain semiconductor amplifier *IEEE J. Quantum Electron.* **28** 842
[71] Hayat A, Nevet A and Orenstein M 2009 Electrically induced two-photon transparency in semiconductor quantum wells *Phys. Rev. Lett.* **102** 183002
[72] Marti D H, Dupertuis M-A and Deveaud B 2003 Feasibility study for degenerate two-photon gain in a semiconductor microcavity *IEEE J. Quantum Electron.* **39** 1066
[73] Nevet A, Hayat A and Orenstein M 2010 Measurement of optical two-photon gain in electrically pumped AlGaAs at room temperature *Phys. Rev. Lett.* **104** 207404
[74] Heatley D R, Firth W J and Ironside C N 1993 Ultrashort-pulse generation using two-photon gain *Opt. Lett.* **18** 628
[75] Kaminski N, Hayat A, Ginzburg P and Orenstein M 2009 Numerical study of few-cycle pulses by nonlinear compression in two-photon semiconductor amplifier *IEEE Photon. Technol. Lett.* **21** 173
[76] Ning C Z 2004 Two-photon lasers based on intersubband transitions in semiconductor quantum wells *Phys. Rev. Lett.* **93** 187403
[77] Valle E, Zippilli S, Laussy F P, Gonzalez-Tudela A, Morigi G and Tejedor C 2010 Two-photon lasing by a single quantum dot in a high-$Q$ microcavity *Phys. Rev.* B **81** 035302
[78] Rong H *et al* 2005 A continuous-wave Raman silicon laser *Nature* **433** 725–8
[79] Shields A J 2007 Semiconductor quantum light sources *Nat. Photon.* **1** 215